ORIGINAL PAPER

Effect of additives on electrodeposition of tin and its structural and corrosion behaviour

R. Sekar · C. Eagammai · Sobha Jayakrishnan

Abstract The present investigation deals with the electrodeposition of tin from chloride electrolytes. Gelatin, β-naphthol, polyethylene glycol, peptone and histidine were used as additives in the plating bath to improve the surface morphology, grain size, smoothness and corrosion resistance of the tin deposits. XRD data obtained for electrodeposited tin show polycrystalline nature with single β-phase and tetragonal structure. A uniform and pore free surface was observed under SEM analysis. AFM results indicate the grain refining brought about by the additives. Corrosion rate measurements using the Tafel extrapolation method and electrochemical impedance spectroscopy reveal the increased corrosion resistance from baths containing additives.

1 Introduction

Tin deposits are widely used in foodstuff processing and canning materials because it is a non toxic, ductile and corrosion resistant metal [1, 2]. Tin is widely used in the electronics industry because of its ability to protect the base metal from oxidation. Tin plating ensures solderability of the base metal, a critical requirement when plating for electronic applications [3].

R. Sekar (✉) · C. Eagammai · S. Jayakrishnan
Electroplating and Metal Finishing Technology Division,
Central Electrochemical Research Institute, Karaikudi 630006,
Tamilnadu, India
e-mail: grsek2004@yahoo.com

Stannous sulphate solutions are mostly used for deposition of tin in the electronic industries, but tin is electrodeposited with low activation polarization from acidic solutions of stannous sulphate in the absence of additives. The deposits obtained under such conditions are porous, coarse and poorly adherent with formation of needles, whiskers and dendrites that cause short circuits between anode and cathode [4–9]. Various organic additives such as surface active agents like cetyl tetraalkyl ammonium bromide, aromatic carbonyl compounds, and amine-aldehyde reaction products, methane sulphonic acid and its derivatives, etc. [10–12] are used in plating solutions. Excess organic additives, higher current density and high metal ion concentration in the plating solution may have a bearing on solderability. Because tin readily forms an oxide, aging will also play a role in the success and failure of the deposit [13]. Kanenk et al. [14] found that the presence of N–N-bis (polyoxyethylene) octadecyl amine in stannous sulphate solution induces a uniform deposition of tin over the whole surface and produces smooth and compact electrodeposits. Fine grained and smooth deposits were obtained from acid stannous sulphate solutions containing some aromatic ketones [15]. It was found that these organic compounds were adsorbed on the cathode surface and enhanced the overpotential. The presence of gluconate ions in the bath improved the quality of the deposits and the throwing power of the bath [16]. Molenaar et al. [17] observed that polyalcohols inhibit the growth of tin crystals in tin autocatalytic deposition.

A review of the literature shows that the electrodeposition of tin from chloride bath has not been investigated in detail and hence this study on effect of additives in chloride bath was taken up. In this paper results on bath characteristics, namely deposition current efficiency and throwing power, and deposit characteristics such as adhesion,

porosity, surface roughness, XRD, SEM, AFM analysis and corrosion resistance of the coatings by potentiodynamic polarization and electrochemical impedance spectroscopy are discussed.

2 Experimental details

The experiments were carried out in triplicate with mild steel specimens. Surface preparation prior to deposition is an important factor and can be achieved by mechanical and electrochemical methods [18–20]. The procedure adopted was removal of surface scales using acid dipping, mechanical polishing to get a smooth surface, degreasing with trichloroethylene and final electrocleaning at 2 A dm^2 in a solution of Na_2CO_3 and NaOH (30 g L^{-1} each). Mild steel panels of 7.5 × 5 × 0.1 cm size were used as cathodes in an electroplating assembly consisting of two 99.99% pure tin anodes on either side of the cathode. The plating bath was operated at 60 °C and at different current densities. The cathodes were weighed before and after deposition and the cathode current efficiency and rate of deposition were calculated. Throwing power was measured using a Haring and Blum cell [21, 22]. This is a rectangular cell consisting of two sheet metal cathodes of 7.5 × 5 × 0.1 cm size filling the entire cross section at both ends, and one perforated anode of the same size. The latter was placed between the cathodes so that its distance from one of the cathode was one-fifth of its distance from the other. Values of throwing power for different solutions used were calculated using Field's formula

Throwing power $(\%) = \dfrac{L - M}{L + M - 2} \times 100$

where M is the metal distribution ratio between the near and far cathode and L is the ratio of the respective distances of the far and near cathodes from the anode.

The bend test by ASTM Test method B571-84 [23] was followed to evaluate the adhesion of the tin coatings. To determine the coating porosity the ferroxyl test was used [24]. This solution consists of sodium chloride (50 g L^{-1}) and white gelatin (50 g L^{-1}), dissolved in distilled water at 45 °C. Filter paper strips of 25 × 25 mm area each were impregnated with the above solution and dried. Before testing the deposit porosity, the filter paper piece was dipped in the above solution and placed at different locations on the plated surface. After 10 min the papers were removed and placed in 10 g L^{-1} solution of potassium ferricyanide. The deposit porosity of was evaluated on the basis of the number of blue spots formed.

Surface roughness was measured using a Surftest SJ-301 surface roughness tester (Mitutoyo, Japan) from the vertical stylus displacement produced during its movement over the surface irregularities.

X-ray diffraction patterns were obtained using the X-pert pro powder diffraction system PE 3040/60 for tin deposits obtained from various tin baths. The deposits produced in the presence of additives and without additives were studied. The samples were scanned at 30–100° (2θ) at a rate of 1 degree per minute using CuK_α ($\lambda = 1.5405$ Å) radiation. The peaks due to the different phases were identified and the corresponding lattice parameters calculated. The crystal size of the tin deposits were calculated using the Scherrer formula [25, 26] from the predominant peak

$$t = \frac{0.9\lambda}{B \cos\theta}$$

where t is the average size of the crystallites, 0.9 is the Scherrer constant, λ is the wavelength of the radiation, B is the peak width at half maximum and θ corresponds to the peak position.

The deposits obtained from different electrolytes were observed visually and by scanning electron microscopy. SEM photographs were taken using the Model JEOL-JSM-35 LF at 25 kV. Molecular imaging atomic force microscopy (AFM) was used in a contact mode with a silicon nitride tip to reveal the 3D surface topography of the deposits.

The polarization behaviour was studied in the test electrolyte for tin deposits of 15 μm thickness. The electrodeposited specimens were masked to expose 1 cm^2 area on one side. A platinum foil (2.5 × 2.5 cm^2) and saturated calomel electrode were employed as auxiliary and reference electrode, respectively; 5% sodium chloride was used as test solution. The working electrode was introduced into the test solution and was allowed to attain a steady potential value. Anodic and cathodic polarization was carried out up to ±200 mV away from the OCP at a scan rate of 1 mV s^{-1}. E_{corr} and I_{corr} values were obtained from the plot of E versus log I curves by the Tafel extrapolation method using an Electrochemical Analyser Model IM6 with THALES software. The same three-electrode cell assembly and instrument was used for the AC impedance measurements. The tin plated samples in the absence and presence of additives were used as working electrode and 5% NaCl solution was used as the test solution. The electrochemical impedance measurements were carried out at open circuit potential in the frequency range from 50 mHz to 100 kHz. The values of solution resistance (R_s), double layer capacitance (C_{dl}) and charge transfer resistance (R_{ct}) were obtained from Nyquist plots of the real (Z_{Re}) versus imaginary ($-Z_{im}$) components of the impedance. The corrosion resistance of the coating was determined from the R_{ct} value, using the Stern–Geary equation [27].

$$I_{corr} = \frac{b_a b_c}{2.303(b_a + b_c)} \frac{1}{R_{ct}}$$

3 Results and discussion

3.1 Current efficiency of deposition

Plating bath compositions, additive concentrations and operating parameters were optimized by preliminary experiments. The bath compositions are given in Table 1 and the operating pH was 4.5–5.5 and the temperature 60 °C. The results of the current efficiency measurements carried out at various current densities are given in Table 2. For bath A, current efficiency decreased with increasing current density above 0.5 A dm^{-2}. This is due to the evolution of hydrogen gas at the higher current densities. It was observed that 0.5–1.0 A dm^{-2} was optimum for producing a smooth uniform satin white deposit with high current efficiency. The result of studies from bath B containing 1.0 g L^{-1} of gelatin as additive shows that the current efficiency increases up to 1.0 A dm^{-2} and thereafter decreases and the quality of the deposit is silvery white to bright silvery white. For bath C containing β-Naphthol the current efficiency gradually increases from 0.25 to 0.5 A dm^{-2} and decreases above 0.5 A dm^{-2}. In general this bath exhibits lower current efficiency, which may be attributed to the fact that this additive is adsorbed at the electrode surface thereby blocking the electrode.

With PEG-6000 in the bath (bath D), light grey deposits were observed at 2.0 A dm^{-2} and smooth uniform satin white deposits at 0.25–1.0 A dm^{-2}, the current efficiency increases up to 1.0 A dm^{-2} and then decreases. In the tin plating bath E with addition of 0.5 g L^{-1} of histidine, matte white deposits were observed at low current density, whereas satin white and silvery white deposits were noted at 1 and 2 A dm^{-2}: the current efficiency decreased with increasing current density.

With addition of 2.0 g L^{-1} peptone (bath F) the current efficiency decreased with increasing current density. Smooth uniform bright satin white deposits were obtained

Table 1 Composition of the baths

Bath	Composition (g L^{-1})	Additive (g L^{-1})
A		Nil
B	Stannous chloride (25)	Gelatin (1.0)
C	Tri sodium citrate (80)	β-Naphthol (1.0)
D	Potassium sodium tartarate (25)	PEG-6000 (1.0)
E	Ammonium sulphate (60)	Histidine (0.5)
F		Peptone (2.0)

Table 2 Current efficiency, rate of electrodeposition and visual appearance of tin electrodeposited from different baths at 60 °C

Bath	Current density (A dm^{-2})	Current efficiency (%)	Rate of deposition (μm h^{-1})	Visual appearance of deposits
A	0.25	92.16	6.70	Satin white
	0.50	98.34	14.30	Satin white
	1.00	90.66	26.38	Bright satin
	2.00	79.65	48.30	Bright satin
B	0.25	73.49	5.36	Silvery white
	0.50	80.42	11.72	Silvery white
	1.00	96.23	28.00	Bright silvery white
	2.00	82.76	50.20	Silvery white
C	0.25	68.67	5.00	Bright satin white
	0.50	78.61	11.44	Bright satin white
	1.00	75.00	21.84	Silvery white
	2.00	67.92	41.20	Silvery white
D	0.25	65.66	4.76	Bright satin white
	0.50	87.95	12.80	Bright satin white
	1.00	92.16	26.82	Bright satin white
	2.00	86.59	52.52	Light gray
E	0.25	90.96	6.60	Matte white
	0.50	85.84	12.48	Matte white
	1.00	79.82	46.46	Satin white
	2.00	65.17	39.52	Bright silvery white
F	0.25	95.78	6.96	Bright satin
	0.50	84.64	12.28	Bright satin
	1.00	79.96	23.28	Bright satin
	2.00	66.97	40.06	Bright silvery white

between 0.25 and 1.0 A dm^{-2} and bright silvery white ones at 2.0 A dm^{-2} with lower current efficiency.

In general additives decreased current efficiency in most of the cases. This can be attributed to the fact that additives may be adsorbed at the electrode surface thereby blocking the surface and decreasing the current efficiency. However, some additives modify the quality of the deposit, probably by incorporation in the deposit and modifying the crystal growth.

3.2 Throwing power

The effect of current density (0.5–2.0 A dm^{-2}) on the throwing power of baths A–F is illustrated in Fig. 1. Throwing power decreases with current density in bath A without additives. The decrease in throwing power with current density is less pronounced in baths B, D and E containing gelatin, polyethylene glycol and histidine. In bath C containing β-Naphthol throwing power increases with current density, while in bath F, containing peptone, it is almost constant. The increased throwing power observed at higher current density for the additive containing baths can be attributed to modification of the potential—current behaviour producing increased cathodic polarization at higher current densities.

3.3 Adhesion and porosity

The coatings neither cracked nor peeled, illustrating good adherence. Ferroxyl tests revealed that deposits from all baths were non-porous at 12 μm thickness.

3.4 Surface roughness

Ra values obtained for the deposit produced from additive free bath was 0.84 μm. Smoother deposits were observed
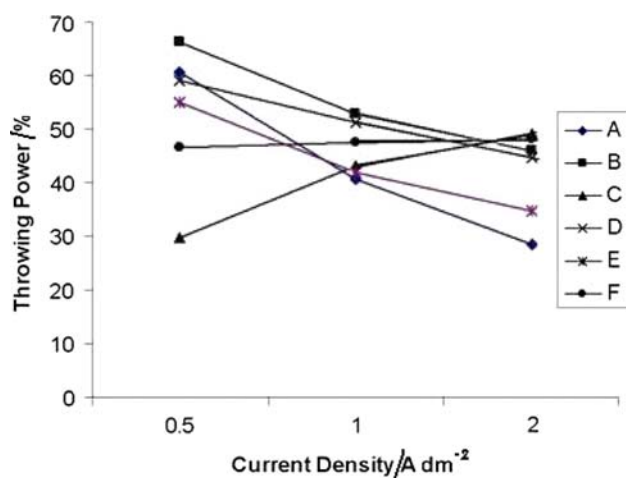
Fig. 1 Effect of current density on throwing power for different baths at 60 °C: (a) bath A, (b) bath B, (c) bath C, (d) bath D, (e) bath E, (f) bath F

in the presence of gelatin and β-Naphthol with Ra values of 0.53 and 0.55 μm, respectively. While incorporation of PEG 6000 produced deposits with Ra 0.98 μm, histidine and peptone give deposits with low Ra values of 0.41 and 0.39 μm, respectively.

3.5 X-ray diffraction studies

The XRD data of the as deposited tin produced from the stannous chloride bath (bath A–F) at 60 °C are shown in Fig. 2a–f. Figure 2a indicate that the deposit from the bath without additives consists of single β-phase with tetragonal structure. The observed 'd' values are in good agreement with the standard values of tin [28]. The peak intensity corresponds to the (220) preferential orientation. XRD data for tin electrodeposited from bath B containing gelatin (Fig. 2b) shows a (220) peak with strong intensity, and the crystal size is decreased in comparison to that of the deposit obtained from the additive free bath (Table 3). This indicates that the texture changed in the presence of the additives [29] and gelatin acts as a grain refiner. Figure 2c shows the XRD pattern of electrodeposited tin from bath C. In this case also a (220) peak with strong intensity was noticed. The other peak intensities are reduced, as reflected in the change in surface morphology of the deposit.

The XRD pattern from the bath containing PEG-6000 (bath D) shown in Fig. 2d shows a (301) diffraction peak with higher intensity and suggests a preferred orientation with the (301) plane parallel to the surface. Similarly in Fig. 2e, the pattern of electrodeposited tin obtained from bath E containing histidine as additive shows preferred orientation with (101) plane parallel to the surface. From Fig. 2f the XRD pattern from bath F, containing peptone as additive, a preferred orientation with the (101) and (002) plane parallel to the surface can be observed and the crystal size calculated using Scherrer formula is 42 nm. Thus it can be seen that peptone reduces the grain size and has a significant effect on the preferred orientation of the deposit, thereby producing smooth bright silvery white deposits of tin.

3.6 Scanning electron microscopy

The morphology and texture of tin coatings are important with respect to susceptibility to whisker growth. The surface morphology of the as deposited tin examined by scanning electron microscopy (SEM) are shown in Fig. 3a–f. Figure 3a shows the deposit produced in the absence of additive (bath A) with block-like crystals and sharp edges on the surface. Figure 3b shows that SEM of electrodeposited tin obtained from bath-B containing gelatin has a more regular and smooth surface morphology, suggesting that the coatings are quite dense with no tendency to dendrite formation. Figure 3c shows the change from block
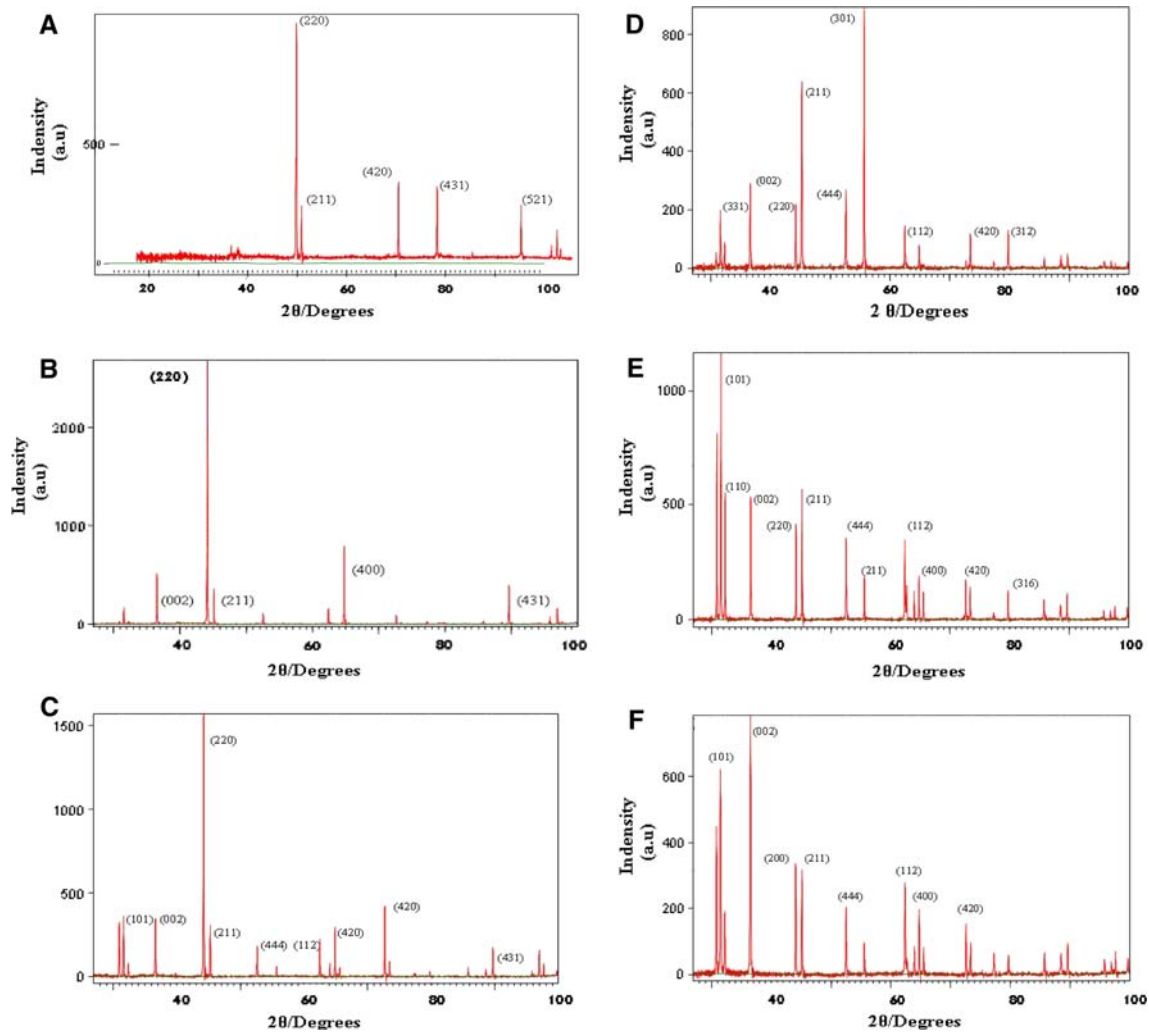
Fig. 2 **a–c** XRD patterns for tin deposit obtained from baths A, B and C. **d–f** XRD patterns for tin deposit obtained from baths D, E and F

Table 3 Crystal size for tin deposits obtained from various baths

Bath	2θ	FWHM 2θ	Plane	Rel. Int. (%)	Crystal size (nm)
A	44.1246	0.0816	220	100	105
B	44.2782	0.1020	220	100	84
C	44.2244	0.1020	220	100	84
D	55.6679	0.1632	301	100	55
E	31.5754	0.1020	101	100	81
F	36.5157	0.2040	002	100	42

grain size into fine grain size showing that β-Naphthol acts as a grain refiner. With addition of polyethylene glycol (PEG-6000) a different surface morphology, Fig. 3d, with block size reduced to fine grain size and characterized by clusters of non-uniform large nodules growing on the surface was observed. Figure 3e shows that on addition of histidine, deposits with a surface morphology with boundaries scattered throughout as clusters of crystals are

produced: the crystal size is decreased in comparison to that for additive free bath A. Figure 3f shows that addition of peptone produced a surface morphology with the block size completely reduced to very fine grained structure suggesting the dense compact nature of the deposits.

3.7 AFM measurements

AFM imaging give a perspective of the 'Z' direction with three dimensional images [30–33]. Figure 4a, the representative AFM scan over an area of 5 × 5 μm, indicates that the deposit obtained from bath A without additive shows the presence of flat mount like structures with no well defined grain boundaries and average grain size of 5 μm.

Figure 4b–f are the AFM images for deposits from baths B to F containing the additives Peak structures with well defined grains and crevices are observed in Fig. 4b and c with grain size 2.6 μm and 1.8 μm, respectively. In Fig. 4d–f homogeneous topography with low dispersion in height

Fig. 3 a–c SEM photograph of tin deposit obtained from baths A, B, and C. **d–f** SEM photograph of tin deposit obtained from baths D, E and F
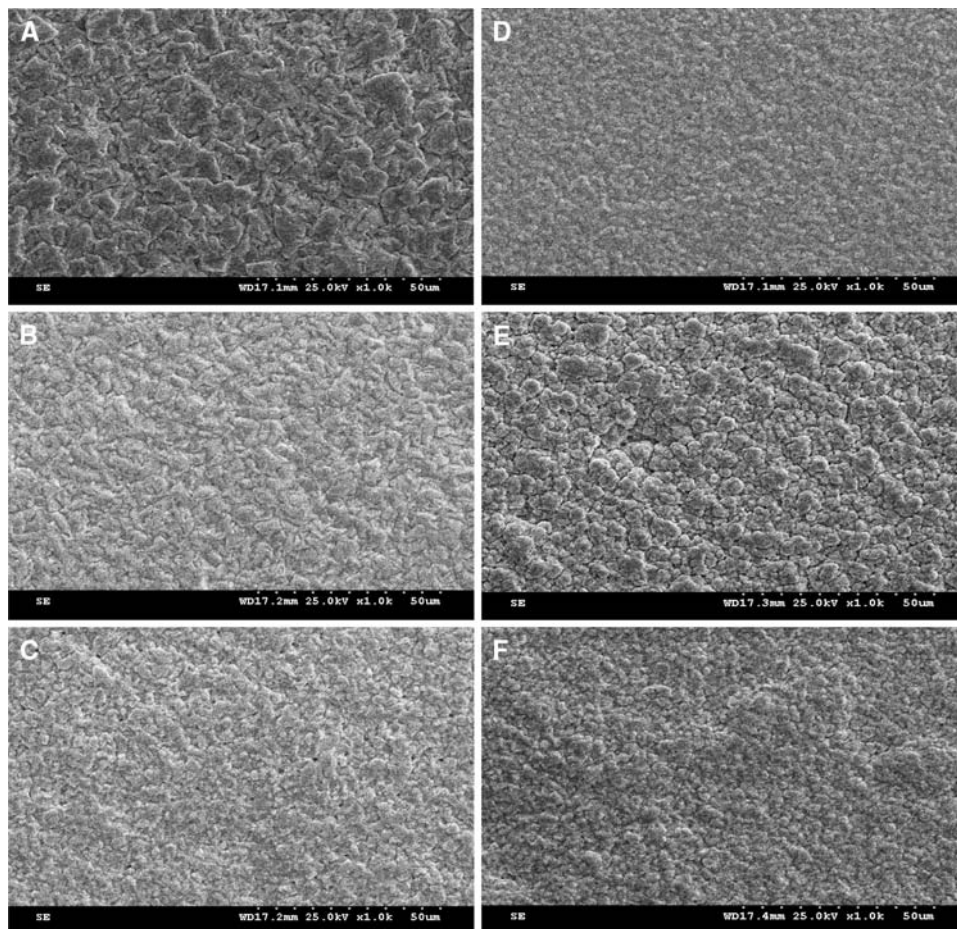
and no predominant peak structure are observed. Grain sizes observed are 0.6 μm, 0.06 μm and 0.02 μm, respectively, from baths containing PEG-6000, histidine and peptone, respectively. These results confirm that the additives studied act as grain refiners with peptone being the best among them.

3.8 Potentiodynamic polarization studies

The parameters derived from E versus log I curves for different tin deposits of 15 μm thickness in 5% NaCl solution are given in Table 4. Figure 5 (curve A) presents the potentiodynamic polarization curve obtained on mild steel with no coating, which exhibits a corrosion potential at more active values and higher corrosion current compared to tin coated steel. Curve B correspond to the deposit produced from bath A; the corrosion potential shifts in the noble direction and the corrosion current is decreased, showing that the tin coating protects the steel substrate from corrosion. Curve C for the deposit obtained from bath B containing gelatin, indicates that the corrosion potential and corrosion current still decrease. This increased corrosion resistance can be attributed to the compact, dense and fine grained nature of the deposit from bath B confirmed from SEM and AFM results.

A similar trend was observed for the deposits obtained from baths C, D, E and F. Among these baths, bath F gave the lowest corrosion current. This indicates that the deposit produced from bath F has the most dense and fine grained structure, which was also clear from SEM and AFM studies.

3.9 Electrochemical impedance spectroscopy (EIS)

The Nyguist impedance diagrams obtained in 5% NaCl solution are shown in Figs. 6 and 7. Curve a shows the diagram for bare mild steel without any coating, curve b for the tin deposit from bath without additive and curves c, d, e, f and g show the EIS for tin deposits from baths B, C, D, E and F with additives.

The impedance plots relevant to the bare mild steel and tin deposits obtained from various baths showed a well defined capacitive loop and there was no evidence of other inductive or capacitive loops at lower frequencies. The corrosion of tin coatings is purely charge transfer controlled, as revealed from the impedance spectrum of perfect semicircle shape [34]. The shape of the impedance spectra supports the assumption that the polarization resistance (R_P) value is the same as the charge transfer resistance (R_{ct}), which is easily estimated on the real impedance axis

Fig. 4 AFM images of tin deposit obtained from baths A, B, C, D, E and F
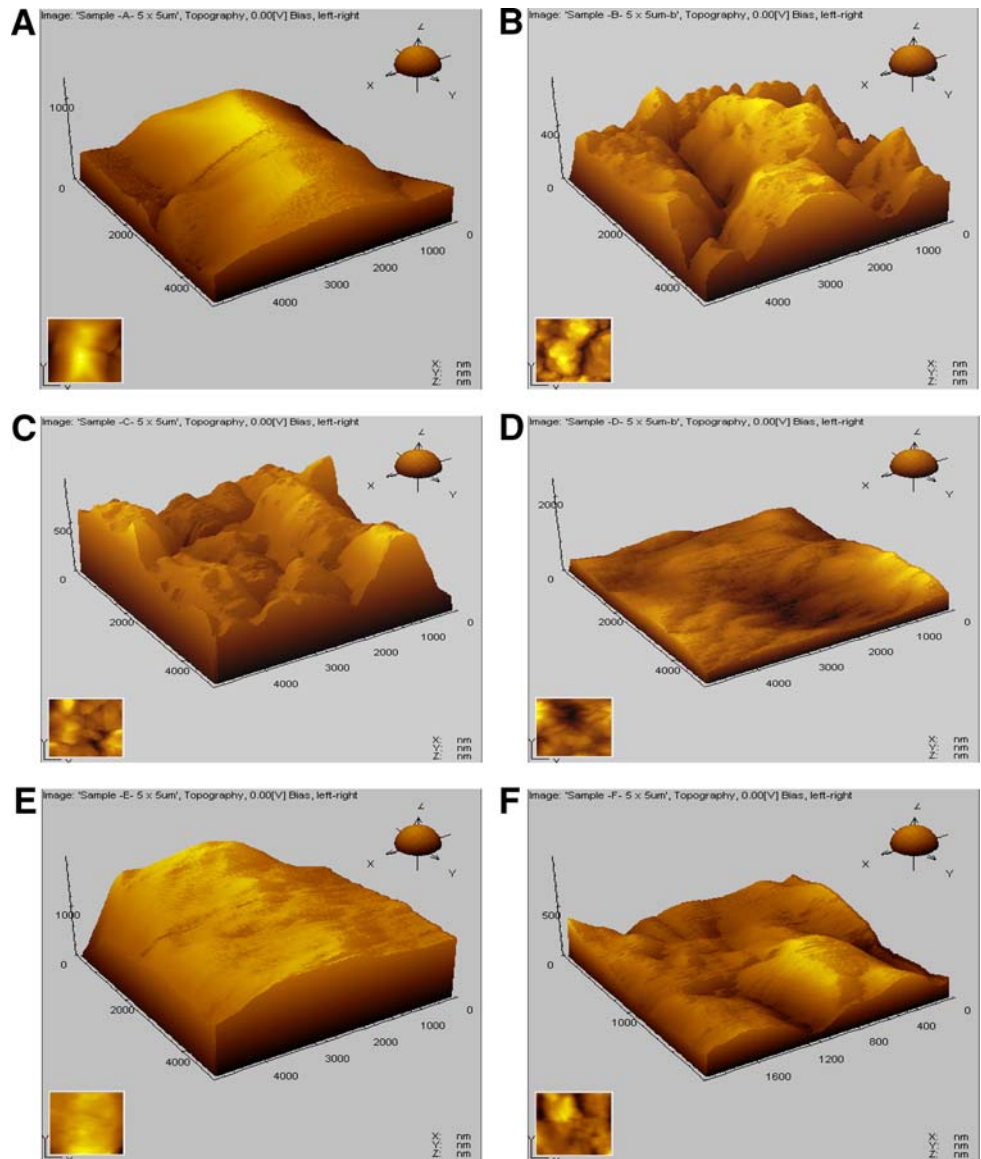
Table 4 Parameters derived from *E*-log *I* curves for tin deposits in 5% NaCl solution

Deposit from bath	Corrosion current (μA cm^{-2})	Corrosion potential (mV versus SCE)	Tafel slopes (mV decade^{-1})	
			Anodic	Cathodic
Bare	2.4	−528	80	31
A	1.5	−510	69	38
B	1.1	−487	52	18
C	1.4	−513	45	15
D	1.3	−504	65	16
E	1.1	−508	92	18
F	0.7	−462	70	40

by extrapolating the impedance trend at the lowest frequencies. Bare mild steel exhibited the lowest R_{ct} value of about 900 mΩ cm^2, whereas the values for baths A, B, C, D, E & F were 11,000, 16,000, 9,000, 11,500, 13,000 & 41,000 mΩ cm^2, respectively. The protective properties of the coatings increase with increasing diameter of the semicircle [35, 36]. Among the six deposits studied, that produced from the bath containing peptone (bath F) produced a larger semicircle with the highest R_{ct} value on the real axis indicating the highest corrosion resistance. This is in clear agreement with microstructural studies indicating that peptone acts as the best grain refiner for the tin coatings from chloride bath.
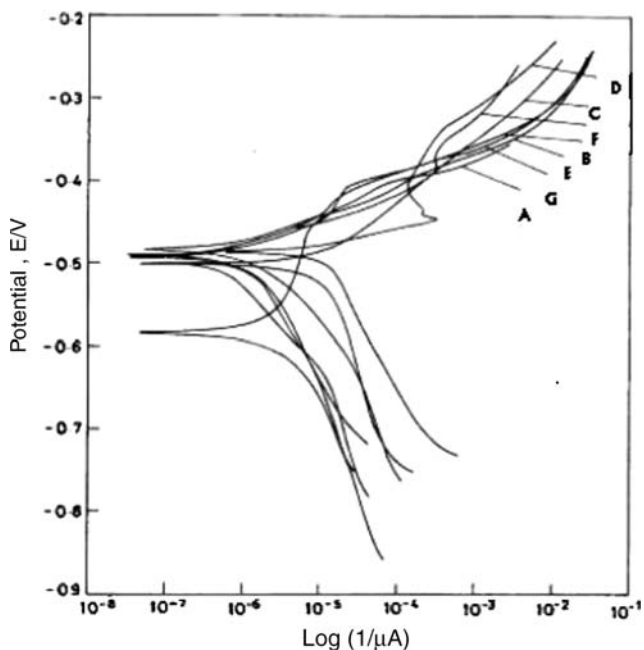
Fig. 5 Potentiodynamic polarization curve for 15 μm tin deposits obtained from different baths in 5% NaCl solution: (a) Bare steel, (b) bath A, (c) bath B, (d) bath C, (e) bath D, (f) bath E, (g) bath F
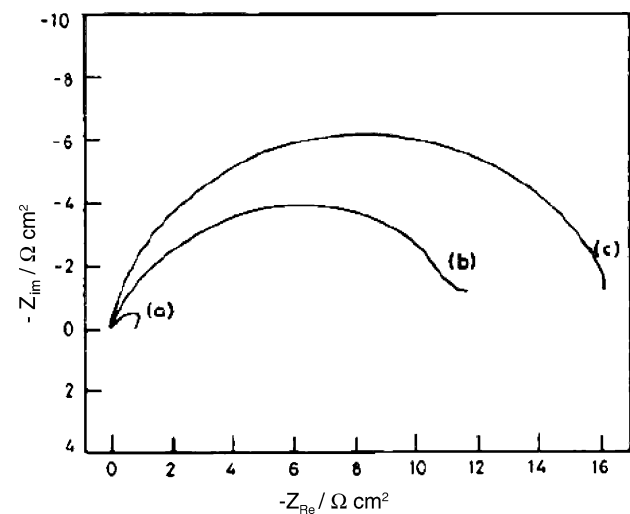
Fig. 6 EIS spectra obtained for various tin deposits (15 μm) in 5% NaCl solution: (a) Bare steel, (b) bath A, (c) bath B, and (d) bath C

4 Conclusion

Smooth and adherent deposits of tin are obtained from chloride based electrolytes with high current efficiency and good throwing power. X-ray diffraction spectra reveal the characteristic XRD pattern of tin but different preferential orientation of lattice planes; the (220) plane is more dominant for deposits from baths A, B, and C, while deposits from baths D, E and F showed the highest reflection of the
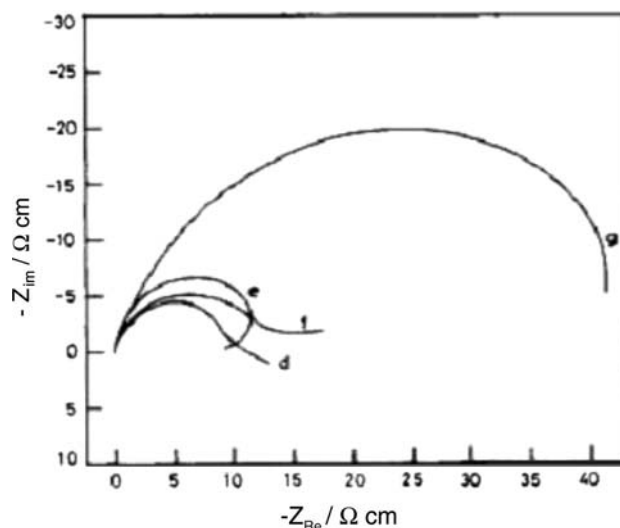
Fig. 7 EIS spectra obtained for various tin deposits (15 μm) in 5% NaCl solution: (d) bath C, (e) bath D, (f) bath E, and (g) bath F

(301), (101) and (002) planes, respectively. The crystal size calculation based on XRD data reveals that the deposit obtained from the peptone containing bath, F, has the smallest crystal size. SEM photographs show that the deposit obtained in the absence of additives has a uniform cluster of block like structures with sharp edges, whereas deposits obtained from the additive containing baths have dense, fine grained, pin hole free structure. AFM analysis reveals the smoothening of three dimensional surface images and the grain refinement brought about by the additives studied, peptone being the best among them.

Potentiodynamic polarization studies reveal the higher corrosion current for deposits obtained in the absence of additives compared to additive containing baths. Among these baths studied, the deposits obtained from the peptone containing bath has the highest corrosion resistance which can be correlated with its dense and fine grained structure. This is further confirmed from the highest R_{ct} value obtained in electrochemical impedance measurements.

References

1. Lowenheim FA (1978) Modern electroplating. McGraw-Hill Book Co, New York
2. Davis PE, Warwick ME, Kay PJ (1982) Plat Surf Finish 6:72
3. Carano M (2000) Plat Surf Finish 87:64
4. Aragon A, Figueroa MG, Gama RE, Zagal JH (1992) J Appl Electrochem 22:558
5. Saba AE, Afifi SE, Sherif AE (1990) Z Phys Chem 167:113
6. Tzeng GS (1995) Plat Surf Finish 82:67
7. Sonoda Y, Nawafune H, Mizumoto S (1992) Plat Surf Finish 79:78
8. Kaneko N, Shinohara N, Nezu H (1991) Electrochim Acta 36:985
9. Kaneko N, Shinohara N, Nezu H (1992) Electrochim Acta 37:2403

10. Martyak NM, Seefeldt R (2004) Trans Inst Met Finish 82:50
11. Martyak NM, Seefeldt R (2005) Trans Inst Met Finish 83:43
12. Kaneko N, Nezu H, Shinohara N, Aoyama T (1985) Denki Kagaku 53:834
13. Carano M (1983) Plat Surf Finish 70:58
14. Kaneko N, Nezu H, Shinohara N (1982) Denki Kagaku 50:659
15. Nakarnura Y, Kaneko N, Nezu H (1994) J Appl Electrochem 24:569
16. Rehim SAE, Sayyah SM, Deeb MME (2000) Plat Surf Finish 87:93
17. Molenaar A, Bakker JW (1989) J Electrochem Soc 136:378
18. Sekar R, Jayakrishnan S (2005) Plat Surf Finish 92:58
19. Sekar R, Kala C, Krishnan RM (2002) Trans Inst Met Finish 80:173
20. Sekar R, Krishnan RM, Muralidharan VS (2004) Trans Inst Met Finish 82:164
21. Silman H, Isserlis G, Averill AF (1978) Protective and decorative coatings for metals. Finishing Publications Ltd, Teddington, England
22. Shawki S, Hanna F, Hamid ZA (1987) Metal Finish 85:59
23. ASTM Test method B571-84 (1995) Adhesion of metallic coatings
24. ASTM Test method B689-81 (1985) Electroplated engineering nickel coatings
25. Cullity BD (ed) (1967) Elements of X-ray diffraction. Addison Wesley Publishing Co Inc, USA
26. Klug HP, Alexander L (eds) (1980) X-ray diffraction procedures for polycrystalline and amorphous materials. Wiley, New York
27. Stern M, Geary AL (1957) J Electrochem Soc 104:56
28. Joint Committee on Powder Diffraction Standards (JCPDS) International Center for Diffraction File PDF-2 Database Sets 1–49 (2000), Pennsylvania
29. Bakkali S, Jazouli T, Cherkaoui M, Tonhami ME (2003) Plat Surf Finish 90:46
30. Barrera E, Palomar MP, Batina N, Gonzalez I (2000) J Electrochem Soc 147:1787
31. Martyak NM, Seefeldt R (2004) Electrochim Acta 49:4303
32. Smith JR, Breakspear S, Campbell SA (2003) Trans Inst Met Finish 81:B26
33. Smith JR, Breakspear S, Campbell SA (2003) Trans Inst Met Finish 81:B55
34. Mansfield F, Kendig W, Tasi S (1982) Corrosion 38:570
35. Survilline S, Cesuniene A, Juskena R (2004) Trans Inst Met Finish 82:18
36. Survilline S, Jasualaitiene V, Cesuniene A (2005) Trans Inst Met Finish 83:130